Physica B 689 (2024) 416174

Contents lists available at ScienceDirect

Physica B: Condensed Matter

journal homepage: www.elsevier.com/locate/physb

Temperature and pressure dependencies of Sm valence in SmB_6 Kondo insulator probed by x-ray absorption spectroscopy

Emin Mijit [a,*], Fabienne Duc [a,*], Olivier Mathon [b], Angelika D. Rosa [b], Gaston Garbarino [b], Tetsuo Irifune [c], Daniel Braithwaite [d], Natalya Shitsevalova [e], Cornelius Strohm [f,*]

[a] Laboratoire National des Champs Magnétiques Intenses, CNRS-INSA-UGA-UPS, F-31400 Toulouse, France
[b] European Synchrotron Radiation Facility, B.P. 220, 38043 Grenoble, France
[c] Geodynamics Research Center, Ehime University, Matsuyama 790–8577, Japan
[d] Université Grenoble Alpes, CEA, Grenoble INP, IRIG, PHELIQS, 38000 Grenoble, France
[e] Institute for Problems of Materials Science, National Academy of Sciences of Ukraine, Krzhyzhanovsky 3, 036 80 Kiev, Ukraine
[f] Deutsches Elektronen Synchrotron, Notkestrasse 85, 22607, Hamburg, Germany

ARTICLE INFO

Keywords:
Kondo insulator
SmB_6
Valence fluctuation
X-ray absorption spectroscopy

ABSTRACT

Pressure and temperature induced valence changes in the Kondo insulator SmB_6 have been investigated using x-ray absorption spectroscopy (XAS) along several isobaric cooling runs and one isothermal compression. The average valence of Sm at various pressure and temperature conditions is extracted from high quality XAS data by peak fitting procedures. The temperature dependence of the Sm valence at ambient pressure shows changes of slope near the known characteristic temperatures of gap formation (120 K) and the in-gap state (50 K). At higher pressures the average valence also shows similar temperature dependent trends upon cooling but the slope changes are less pronounced. This behavior is discussed in relation to the possible existence of an underlying first order valence transition and its critical end point. At constant temperature ($T = 20$ K), the Sm valence increases rapidly with pressure; however, it remains far below the expected integer value (3+) near the onset of the magnetic ordering and gap closure. In addition, the local structure of SmB_6 at ambient conditions has been analyzed using extended x-ray absorption fine structure.

1. Introduction

Strong electronic correlations in the rare-earth based *f* electron compounds give rise to a variety of interesting behaviors, including quantum criticality, unconventional superconductivity, heavy fermions and non-Fermi liquid states. In recent years, critical valence fluctuations and valence transitions have attracted growing attention as a key ingredient for understanding those unusual phenomena [1–3]. In many Ce and Yb-based heavy fermion compounds, optimal superconductivity or quantum critical point occurs at the pressure of a valence crossover, which arises from a virtual critical end point (CEP) of an underlying first order valence transition [1–3].

The intermediate valence compound SmB_6 has been extensively studied in the past as a prototypical Kondo insulator [4,5], and experienced tremendous renewed interest in recent years for its topologically protected metallic surface state [6,7]. At ambient temperature, SmB_6 behaves like a correlated poor metal but undergoes a metal to insulator crossover at lower temperatures [4]. The opening of a gap in SmB_6 with decreasing temperature is associated with the Kondo effect, a many-body interaction process between the local magnetic moments and itinerant conduction electrons [8]. At temperatures below the Kondo coherence temperature, strong hybridization of the itinerant *5d* electrons and low lying local *4f* states in SmB_6 give rise to a narrow hybridization gap of the order of 10–20 meV [9,10]. With the chemical potential lying within this hybridization gap, the material is effectively in an insulating (semiconducting) phase [5]. At temperatures below 40 K, an in-gap resonance state emerges due to collective excitations of magnetic origin with the presence of spin–orbit coupling and valence fluctuations [11,12]. The ground state of SmB_6 changes drastically under high pressure, the insulating gap closes around $P_c \approx 4$–10 GPa showing also a simultaneous magnetic ordering below 12 K [13–15].

Any change in the *4f-5d* hybridization modifies the occupancy of the $4f$ shell, and leads to changes in the ratio of fluctuating $4f^6$ (Sm^{2+}, $J = 0$) and $4f^5$ (Sm^{3+}, $J = 5/2$) configurations. Accurate measurements of the Sm valence (a measure of the degree of localization and the total angular momentum) under different thermodynamic conditions are therefore crucial for the understanding of the various novel phases and

* Corresponding authors.
E-mail addresses: emin.mijit.17@gmail.com (E. Mijit), fabienne.duc@lncmi.cnrs.fr (F. Duc), cornelius.strohm@desy.de (C. Strohm).

https://doi.org/10.1016/j.physb.2024.416174
Received 21 February 2024; Received in revised form 29 May 2024; Accepted 3 June 2024
Available online 6 June 2024

transitions occurring in SmB_6. Indeed, the average valence of Sm (υ_{Sm}) in SmB_6 has been determined by several studies based on core level X-ray spectroscopy techniques such as x-ray photoelectron spectroscopy (XPS) [16–18] and x-ray absorption spectroscopy (XAS) [19–23], reporting ambient pressure values within the range $\upsilon_{Sm} = 2.59 - 2.7$ [16,17,21] at room temperature and $\upsilon_{Sm} = 2.48 - 2.55$ at low temperatures (4–10 K) [17,18,21,22]. In addition to the differences in the absolute values, the reported temperature dependencies of υ_{Sm} appear to follow different trends [17,19,21,22], even if the same spectroscopy technique was used [19,21,22].

In this work, we studied the pressure effects on the temperature dependence of υ_{Sm} to investigate the possible correlation between Kondo insulating behavior and critical valence fluctuations (associated with a CEP) in SmB_6. We focused our attention on the low-pressure range of the phase diagram where the temperature induced valence changes are significant. The temperature dependence of υ_{Sm} at ambient pressure has been revisited, and compared to the behavior at higher pressure (new measurements at 1.0 and 2.0 GPa). The average valence at various temperature and pressure points has been estimated by careful analysis of the Sm L_3−edge XAS spectra. Differences in the temperature dependence of υ_{Sm} at different pressures are discussed. In order to understand the evolution of υ_{Sm} towards the onset of gap-closure and magnetic ordering, we also measured its pressure dependence along an isotherm at 20 K. Additionally, we investigated the local structure of SmB_6 at ambient conditions using x-ray absorption fine structure (EXAFS) technique.

2. Experiments

High purity SmB_6 was initially synthesized in powder form by routine boron-thermal reduction of samarium oxide (Sm_2O_3) in vacuum at 1650 °C. The purity of Sm_2O_3 was 99.998%, and that for boron enriched with the ^{11}B isotope was more than 99.99%. The obtained powder was pressed in the form of a rod, which was sintered at 1750 °C in a vacuum and used for further growth of the SmB_6 single crystal by the method of crucibleless induction zone melting under high purity argon pressure. The crystal was remelted three times before obtaining the final high quality single crystal.

Pressure and temperature dependent XAS measurements were performed at the BM23 beamline of the European Synchrotron Radiation Facility (ESRF) [24]. A double crystal monochromator equipped with two Si(111) crystals in fixed exit geometry was employed to monochromatize the incoming beam and scan the energy. The x-ray beam was focused down to 3×3 μm^2 using two Platinum coated mirrors in Kirkpatrick–Baez (KB) geometry. Higher order harmonics were rejected by setting these mirrors to an incidence angle of 7.0 mrad. XAS spectra were measured in transmission mode (in axial geometry through the diamond anvils) scanning across the Sm L_3-edge. High pressures up to 8 GPa and low temperatures down to 10 K were achieved by a diamond anvil cell which was mounted inside a helium flow cryostat. In order to avoid glitches on the XAS spectra (single crystal diamond anvils introduce glitches on the XAS spectra at x-ray energies where a Bragg condition is satisfied, because the diffracted intensity does not reach the detector and the normalization fails), the diamond anvil cell was equipped with nano-polycrystalline diamond (NPD) anvils [25,26] of 600 μm culet size. One of the anvils was partially perforated to reduce its absorption (total thickness of two diamonds was 1.75 mm). For the preparation of the diamond anvil cell, a 150 μm thick stainless steel gasket was pre-indented to a final thickness of 70 μm and laser drilled to obtain a sample chamber of about 300 μm diameter. A rectangular piece of uniformly polished SmB_6 single crystal with 20 μm thickness was loaded into the sample chamber, together with a tiny ruby sphere for pressure determination. The rest of the sample chamber was filled with silicon oil which served as pressure transmitting medium (PTM). Use of gas PTMs was avoided to prevent the failure of the cell with perforated NPD anvil, because PTMs like He can easily penetrate into the micro-structures of NPD diamonds (it can happen also with neon depending on the quality of such diamonds). The pressure was determined from the pressure and temperature dependent shift of the ruby fluorescence spectra [27]. Sample pressure was monitored frequently (at each temperature) during the isobaric cooling runs, and kept constant at nominal values by regulating the membrane pressure. No sign of non-hydrostaticity was observed from the ruby fluorescence spectra during these cooling runs. In fact, non-hydrostatic effects of silicon were reported to be negligible even at low temperature (77 K) for $P \leq 2.0$ GPa [28].

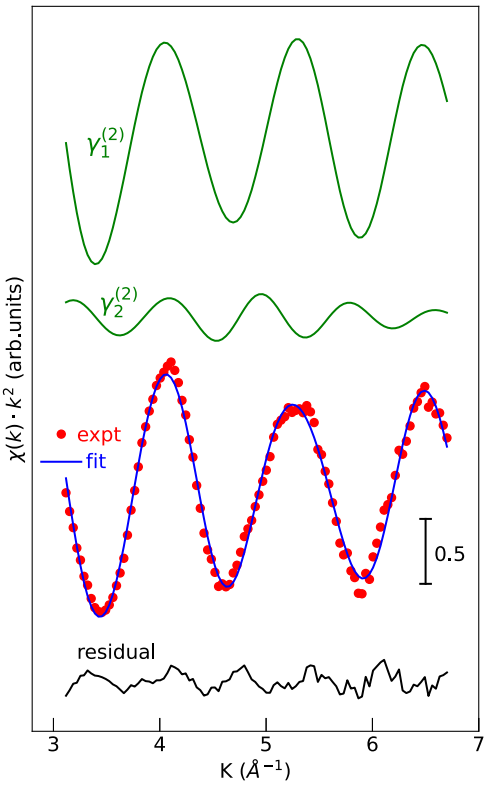

Fig. 1. A typical EXAFS refinement performed for Sm L_3-edge EXAFS data measured under ambient conditions (1 bar, 300 K). The original XAS spectrum from which we extracted this EXAFS signal is given in Fig. S1 (SI file). Best-fit theoretical signal includes two two-body correlations from first ($\gamma_1^{(2)}$) and second ($\gamma_2^{(2)}$) coordination shells.

3. Results and discussion

3.1. EXAFS analysis at ambient conditions

Previous EXAFS investigations on mixed valence compounds have explored possible evidence of distorted local structures with different nearest neighbor distances corresponding to different valence state of the rare-earth ion [29–31]. However, most of the these earlier EXAFS studies have concluded that the nearest neighbor shell surrounding the rare-earth cation adopts an average distance. We measured Sm L_3-edge XAS data in a wide energy range (up to 600 eV above the edge) to verify the validity of this conclusion in SmB_6. Thanks to the NPD anvils, Sm L_3-edge XAS data could be measured without strong spurious glitches, especially in the x-ray absorption near edge structure (XANES) range where the peak fitting procedures is performed for quantitative valence analysis. However, the presence of some distortions in the higher energy post-edge range could not be avoided due to the single crystalline nature of the sample itself (see Fig. S1 in the SI file). Exploitable EXAFS could only be obtained for a few data sets. Here, we provide an example EXAFS refinement for the data measured at ambient conditions. As

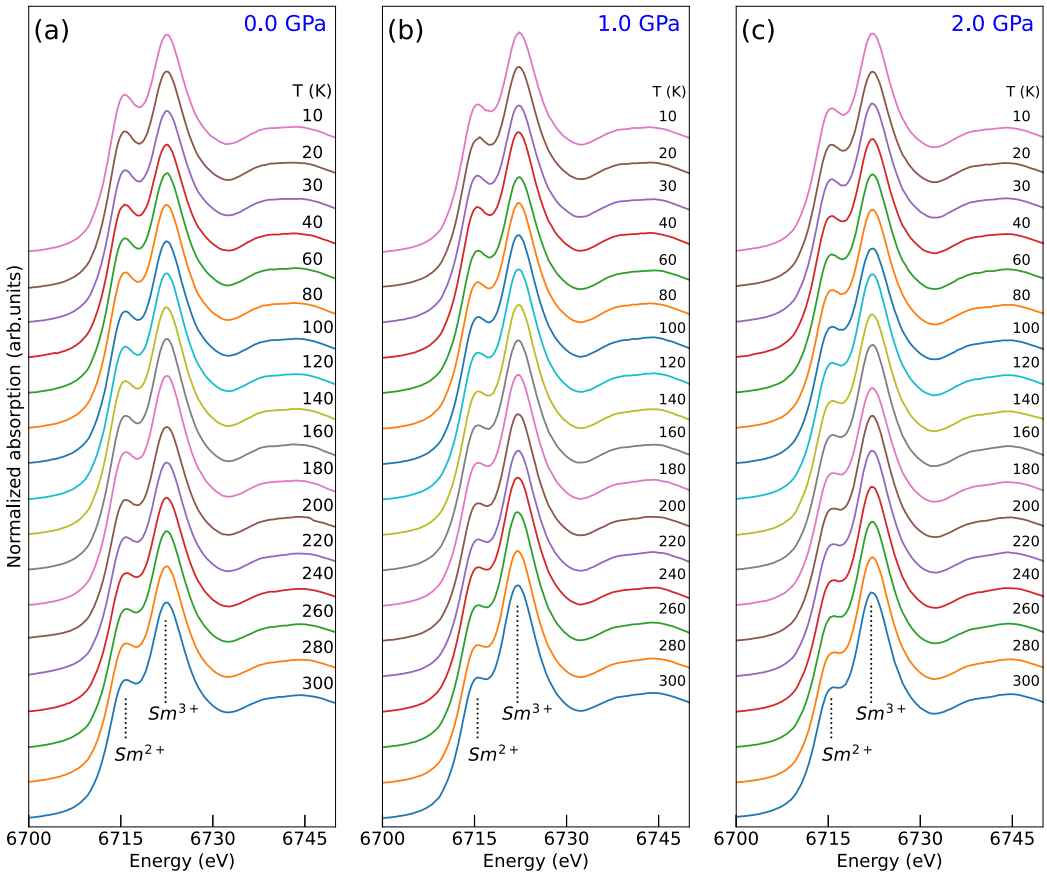

Fig. 2. Temperature dependent Sm L_3-edge XAS data measured along cooling runs at 0.0 GPa (a), 1.0 GPa (b) and 2.0 GPa (c).

shown in Fig. 1, experimental Sm L_3-edge EXAFS signal of SmB_6 measured at ambient conditions was refined including two two-body correlations from first ($\gamma_1^{(2)}$) and second ($\gamma_2^{(2)}$) coordination shells. The fit was performed using the GNXAS program [32,33], by varying the atomic distances and disorder parameters concerning the first shell Sm-B and second shell Sm-Sm distributions. The coordination numbers (CN) associated with individual two-body correlations were fixed to the known values of $CN_1 = 24$ and $CN_2 = 6$ (fitting these well known numbers is not justified, considering also the short k range of the data). The agreement between the fit and the experimental data is shown in Fig. 1. From the EXAFS refinement, best-fit structural parameters such as the first shell Sm-B atomic distance $R_1 = 3.046(5)$ Å, the second shell Sm-Sm distance $R_2 = 4.12$ (1) Å, and the corresponding disorder parameters $\sigma_1^2 = 0.004(2)$ Å^2 and $\sigma_2^2 = 0.036(10)$ Å^2 have been obtained. Values of atomic distances obtained here are in agreement with the calculated values using crystallographic parameters reported from previous diffraction studies [19,34,35].

3.2. Temperature dependent XAS

X-ray absorption spectroscopy is highly sensitive to the valence state and electronic configuration of elements in materials of various composition [36–38]. It has been widely used as a standard tool for the studies of valence fluctuating compounds [19,21,22,39,40]. The XANES range of the normalized temperature dependent Sm L_3-edge XAS spectra measured along isobaric cooling runs at 0.0, 1.0 and 2.0 GPa are shown in Fig. 2 (a–c). In this figure, the white line range (6710–6730 eV) of each individual spectrum consists of two components, typical of mixed valence compounds. As indicated in Fig. 2(a), the shoulder like peak at the lower energy side (~6715 eV) corresponds to the divalent Sm^{2+} component (with $4f^6 5d^0$ configuration), while the stronger peak at the high energy side (~6722 eV) corresponds to the trivalent Sm^{3+} state (with $4f^5 5d^1$ configuration). One can see from Fig. 2 that the relative intensity of the Sm^{2+} peak increases upon cooling at the expense of Sm^{3+} component, indicating a more stabilized Sm^{2+} state at low temperatures. In order to quantitatively determine the average valence of Sm, the spectral weights of Sm^{2+} and Sm^{3+} configurations have been evaluated by a peak fitting procedure. Each spectral component was modeled by the sum of a Lorentz and arctangent functions to mimic the peak shape and corresponding edge jump, respectively. The spectral line shape is then fitted by the following model:

$$f(E) = \sum_{i=2}^{3} \Big[\frac{A_i(\gamma_i/2)}{(E-E_i)^2 + (\gamma_i/2)} + \frac{A_i\gamma_i}{A_2\gamma_2 + A_3\gamma_3} \{ \frac{1}{2} + \frac{1}{\pi} \arctan \frac{E - E_i - \delta}{\Gamma_i/2} \} \Big]$$

Here, suffix $i = 2$ and $i = 3$ represent the divalent and trivalent terms, E_i, A_i and γ_i are the energy position, intensity and full width at half maximum of the Lorentzian peaks, while Γ_i is the broadening term for the arctangents. The parameter δ is used to account for a possible slight energy shift of the continuum states of the two individual components. In this model, ratio of the white line intensity and edge jump is assumed to be equal for Sm^{2+} and Sm^{3+} configurations (around 10% of difference is approximated if one counts only the number of empty 5d holes in the final state). Nevertheless, such model functions are widely used to determine the rare-earth valence in *4f* electron compounds [19–23,41]. Using the best-fit A_i and γ_i parameters, υ_{Sm} is given by the weighted area of the two components using the relation:

$$\upsilon = 2 + \frac{A_3\gamma_3}{A_2\gamma_2 + A_3\gamma_3}$$

The initial fit was performed for the spectrum measured at ambient conditions, relaxing all parameters mentioned above. The resulting value $\upsilon_{Sm} = 2.60(1)$ from this fit is in good agreement with those

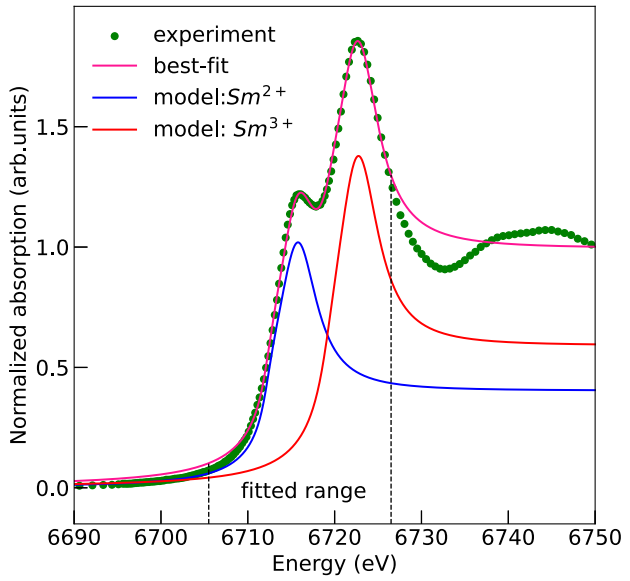

Fig. 3. A typical fit (pink line) performed on a normalized Sm L_3-edge XAS spectrum (green circles) measured at $P = 2.0$ GPa and $T = 20$ K. Fitted spectral energy range is indicated by two vertical dashed lines.

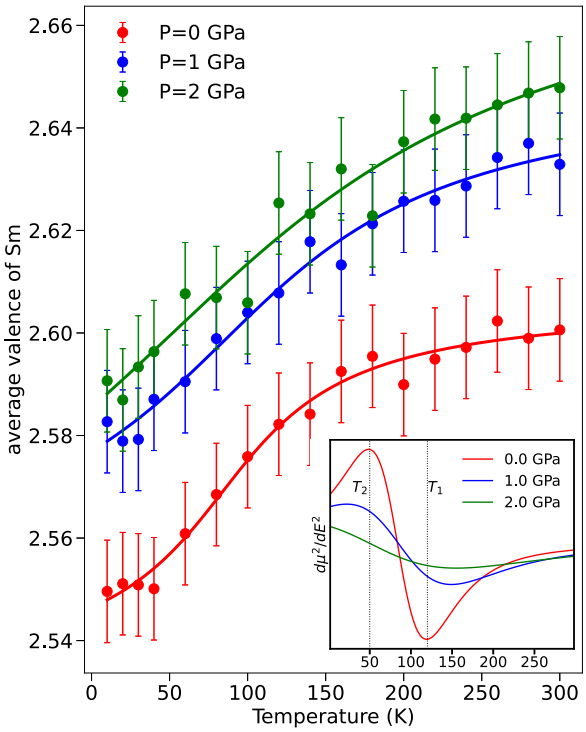

Fig. 4. Average Sm valence derived from the T dependent XAS data shown in Fig. 2. Solid line curves are guide for the eyes, obtained by fitting the data points using a arctangent function. The inset shows second derivatives of valence vs. temperature curves (solid lines) of the main figure.

obtained by most of the previous XAS measurements [19,21,22]. In order to perform a more consistent analysis of all data sets, spectra at other temperature and pressure points were fitted by relaxing A_2 and A_3 as fitting parameters, and fixing the rest of the parameters at their value at ambient conditions. Peak positions (E_2 and E_3) were relaxed (within a narrow range) at high pressures, to account the slight energy shift of spectral features induced by reduced inter-atomic distances.

A typical fit performed on a spectrum measured at $P = 2.0$ GPa and $T = 20$ K is shown in Fig. 3. Fig. 4 shows the temperature dependence of the average Sm valence at 0 GPa, 1.0 GPa, and 2.0 GPa obtained by fitting the data sets (in Fig. 2) with the procedures described above. At ambient pressure, the average valence and its temperature dependence are in agreement with those reported by Mizumaki et al. and Chen et al. for $T > 120$ K [21,22], while our values deviate at lower temperatures (see the comparison from Fig. S2 in the supplementary file). On the other hand, the values for the valence obtained in this work for $T < 50$ K are close to those reported by Utsumi et al. [17]. Discrepancies of the values from different studies can possibly be attributed to systematic differences in the experimental techniques (e.g. x-ray photoemission in Ref. [17], dispersive XAS in Ref. [22], and standard XAS in this work and Ref. [21]), fitting procedures and differences in the sample (quality and form, see supplementary information). Nevertheless, the trend of temperature dependent changes in υ_{Sm} at ambient pressure is in qualitative agreement with earlier work reported by Mizumaki et al. [21], showing changes of slope at two characteristic temperatures around $T_1 \approx 120$ K and $T_2 \approx 50$ K (indicated by dashed vertical lines in Fig. 4). Characteristic temperatures T_1 and T_2 here are defined according to the maximum and minimum peaks in the second derivative of υ_{Sm} vs. T curves, as shown in the inset of Fig. 4 and Fig. S3 (supplementary file).

At ambient pressure, υ_{Sm} decreases slowly upon cooling until $T_1 \approx 120$ K. Below T_1, υ_{Sm} decreases more rapidly upon further cooling down to $T_2 \approx 50$ K, reflecting a more quick hybridization process between localized *4f* and conducting *5d* states (favoring the $4f^6$-like configuration). Below $T_2 \approx 50$ K, the average valence is nearly temperature independent, stabilizing around a value of about $\upsilon_{Sm} = 2.55(1)$, until 10 K (the lowest temperature reached in this work). The temperature onset of the rapid valence change ($T_1 \approx 120$ K) is consistent with the known Kondo coherence temperature, and the temperature onset of the semiconducting phase [9,10,42,43], demonstrating the intimate correlation between the changes in the Sm valence (hybridization of *4f* and conduction states) and the formation of the Kondo gap at the Fermi level [10,42]. While, the other characteristic temperature $T_2 \approx 50$ K, below which the valence remains stable, coincides with the temperature onset (~40 K) of the in-gap state observed by Raman scattering and scanning tunneling spectroscopy measurements [11,12]. Nearly constant non-integer values of υ_{Sm} (≈2.55) below $T_2 \approx 50$ K indicate that SmB_6 is within valence fluctuating regime also at low temperatures well below the gap formation and in-gap state.

At higher pressures of 1.0 and 2.0 GPa, υ_{Sm} also decreases upon cooling, but starting from higher room temperature values of $\upsilon_{Sm} = 2.63$ and $\upsilon_{Sm} = 2.65$, respectively. However, changes of slope (around T_1 and T_2) seem to be suppressed with the increase of pressure, changing to an almost monotonic decreasing trend at 2.0 GPa. The metal–insulator transition (MIT) in SmB_6 is known to occur within 4–10 GPa range depending on the experimental conditions [13–15]. Under quasi-hydrostatic conditions (e.g, when a solid PTM like NaCl is used), MIT occurs at lower pressures (as low as 4.0 GPa) [15]. The onset pressure of the MIT is pushed up to 10 GPa in case of hydrostatic experiments [14]. The liquid PTM (silicon oil) that we used in this study was reported to be hydrostatic below 2.0 GPa at 77 K [28]. Thus development of considerable deviatoric stress is not expected from our cooling runs at constant pressures. Therefore, less pronounced slope changes (between 50–120 K) in the valence vs. T curves that we observed here are not related with the MIT or with pressure in-homogeneity. Instead, this behavior is reminiscent of what happens in the typical Ce, Yb and Eu valence transition systems (e.g. elemental Ce metal, $YbInCu_4$ and $EuRh_2Si_2$) which show sharp valence transitions at lower pressures but move to a gradual valence crossover regime under physical or chemical pressure [44–49]. For example, in the case of Ce metal, the valence change and thus the decrease of the volume become more continuous upon cooling at pressures higher than 2.0 GPa, after escaping from the pressure–temperature ranges of the $\gamma - \alpha$ transition line and its CEP

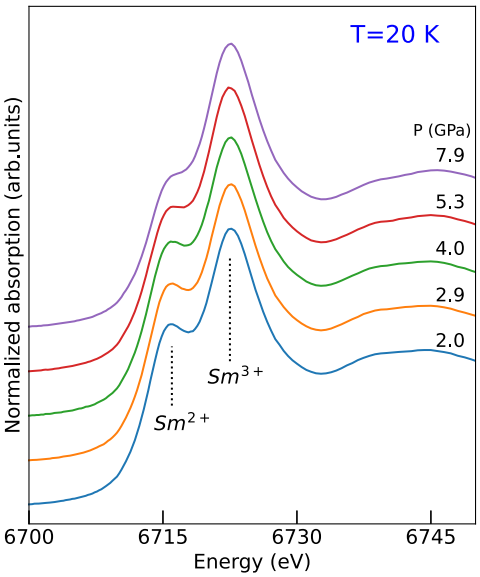

Fig. 5. Pressure dependence of Sm L_3-edge XAS spectra measured along the isotherm at 20 K.

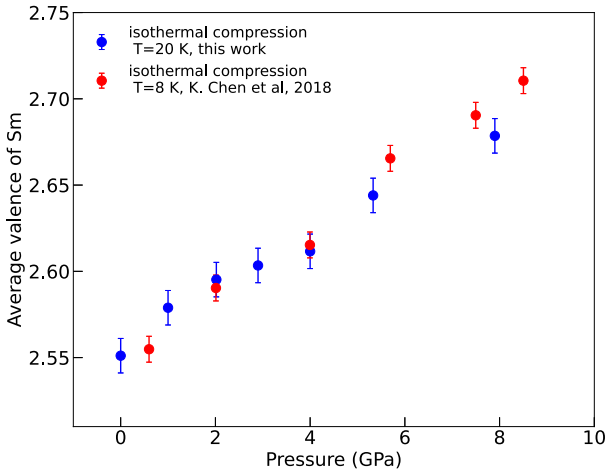

Fig. 6. Pressure dependence of the average Sm valence (at 20 K) obtained from this work compared with the pressure dependent Sm valence (at 8 K) reported in Ref. [22].

(at about 600 K and 2.0 GPa) [44,45]. Similar behavior also occurs in compounds like $YbInCu_4$ and $EuRh_2Si_2$, where the temperature dependent valence change becomes more continuous under physical or chemical pressure, after exceeding the domain of the existing CEP [46–49]. The existence and location of such a CEP plays a decisive role for the emergence of various exotic phases in valence fluctuating and heavy fermion compounds (such as unconventional superconductivity) [1–3]. We therefore can speculate that the gap formation and Kondo insulator behavior in SmB_6 is also associated with an underlying first order valence transition. If this is the case, the underlying CEP would be expected to be located at negative pressures due to the fact that the observed anomalies in the temperature dependent valence change at ambient pressure are still not very sharp. In addition, no drastic volume change (characteristic of first order valence transitions) was observed in SmB_6 at ambient pressure. In fact, the possible existence of such an underlying first order phase transition and CEP was also discussed and proposed by a recent theoretical work [50].

3.3. Pressure dependent XAS

Several pressure dependent Sm L_3-edge XANES spectra measured along the 20 K isotherm are shown in Fig. 5. The application of pressure stabilizes the Sm^{3+} state as indicated by the increased weight of the Sm^{3+} at the expense of Sm^{2+} peak. The pressure dependence of v_{Sm} was evaluated using the peak fitting procedure described above. For this set of high pressure data, E_2 and E_3 were relaxed with minor freedom in addition to the fitting parameters A_2 and A_3. This was necessary to account for the pressure induced shift of the resonance peaks introduced by the decrease of atomic distances (energy position of the XAS resonance peaks is inversely proportional to the square of atomic distances, according to Natoli's rule: $(E_{peak} - E_{edge}) \cdot R^2 = constant$ [51]).

In Fig. 6, the average Sm valence v_{Sm} is plotted as a function of pressure. As we can see, the pressure dependence of v_{Sm} and its absolute values obtained in this work are in agreement with those obtained by Chen et al. at 8 K [22]. The trend of v_{Sm} upon compression is similar to the behavior observed at room temperature [52], but very different from the result of another room temperature measurement (in which v_{Sm} increase rapidly above 4.0 GPa and approaches to 3.0 around 8–10 GPa) [15]. Possibly, such disagreement originated from the employment of different pressure mediums (NaCl vs. silicon oil) and fitting procedures (one arctangent function instead of two) used in (Ref. [15]). From our data, v_{Sm} increases upon compression without noticeable anomaly, and reaches a value of $v_{Sm} \approx 2.670(5)$ at 8.0 GPa. The increase of valence, and thus the Sm^{3+} configuration with angular momentum $J = 5/2$ is in line with the non-magnetic to magnetic transition accompanied by gap closure in 6–10 GPa pressure range [13,14]. However, the $v_{Sm} \approx 2.70(1)$ at a pressure near the magnetic transition pressure remains far below the integer value (3+). This is markedly different from the typical valence fluctuating compounds which favor a *4f* electron configuration with near integer valence in the high pressure magnetic phase [53–57]. These results are in agreement with findings reported in previous high-pressure experiments on SmB_6 [23,52].

4. Conclusion

In summary, we have investigated the pressure and temperature induced valence changes in the Kondo insulator SmB_6 along several isobaric cooling runs and an isothermal compression using XAS. The average valence of Sm at various pressure and temperature conditions have been extracted from high quality XAS data by peak fitting procedures. The changes of slope in the temperature dependence of v_{Sm} were discussed in relation with the formation of the hybridization gap and in-gap states. Differences in the v_{Sm} versus temperature curves at different pressures were discussed in relation to an underlying first order valence transition. We suggest that the critical end point of this first order valence transition would be located at negative pressures. The pressure dependence of the Sm valence along the isotherm at 20 K has shown that v_{Sm} is far below the expected value of +3 near the pressure onset of the long range magnetic ordering. The local structure of SmB_6 at ambient conditions was studied using EXAFS signals. We extracted values for radial distribution of the first and second coordination shells. These values (especially atomic distances) are in agreement with the results of previous diffraction experiments. A more profound temperature and pressure dependent EXAFS study (using powder samples) would be desirable in order to better quantify the local structural changes associated with the gap formation and valence fluctuations in SmB_6.

CRediT authorship contribution statement

Emin Mijit: Writing – review & editing, Writing – original draft, Visualization, Methodology, Investigation, Formal analysis, Data curation. **Fabienne Duc:** Writing – review & editing, Writing – original draft, Validation, Supervision, Methodology, Investigation, Funding acquisition, Formal analysis, Data curation, Conceptualization. **Olivier**

Mathon: Methodology, Investigation. **Angelika D. Rosa:** Methodology, Investigation. **Gaston Garbarino:** Methodology, Investigation. **Tetsuo Irifune:** Resources. **Daniel Braithwaite:** Resources. **Natalya Shitsevalova:** Resources. **Cornelius Strohm:** Writing – review & editing, Writing – original draft, Visualization, Validation, Supervision, Methodology, Investigation, Formal analysis, Data curation, Conceptualization.

Declaration of competing interest

The authors declare that they have no known competing financial interests or personal relationships that could have appeared to influence the work reported in this paper.

Data availability

Data will be made available on request.

Acknowledgments

We acknowledge European Synchrotron Radiation Facility (ESRF), France for the provision of beam-times (in-house) at the BM23 beamline. We thank Andrea Di Cicco (University of Camerino, Italy) and Fabio Iesari (University of Toyama, Japan) for their advices during the data analysis. The authors also acknowledge the support from ISABEL project, funded by the European Union's Horizon 2020 research and innovation programme (Grant Agreement No. 871106).

Appendix A. Supplementary data

Supplementary material related to this article can be found online at https://doi.org/10.1016/j.physb.2024.416174.

References

[1] G.W. Scheerer, Z. Ren, S. Watanabe, G. Lapertot, D. Aoki, D. Jaccard, K. Miyake, The dominant role of critical valence fluctuations on high Tc superconductivity in heavy fermions, Npj Quantum Mater. 3 (41) (2018) 41.

[2] S. Watanabe, K. Miyake, Quantum valence criticality as an origin of unconventional critical phenomena, Phys. Rev. Lett. 105 (2010) 186403, http://dx.doi.org/10.1103/PhysRevLett.105.186403, URL https://link.aps.org/doi/10.1103/PhysRevLett.105.186403.

[3] S. Watanabe, K. Miyake, Roles of critical valence fluctuations in Ce-and Yb-based heavy fermion metals, J. Phys.: Condens. Matter. 23 (9) (2011) 094217.

[4] A. Menth, E. Buehler, T.H. Geballe, Magnetic and semiconducting properties of SmB_6, Phys. Rev. Lett. 22 (1969) 295–297, http://dx.doi.org/10.1103/PhysRevLett.22.295, URL https://link.aps.org/doi/10.1103/PhysRevLett.22.295.

[5] P.S. Riseborough, Heavy fermion semiconductors, Adv. Phys. 49 (3) (2000) 257–320.

[6] M. Dzero, K. Sun, V. Galitski, P. Coleman, Topological Kondo insulators, Phys. Rev. Lett. 104 (2010) 106408, http://dx.doi.org/10.1103/PhysRevLett.104.106408, URL https://link.aps.org/doi/10.1103/PhysRevLett.104.106408.

[7] S. Wolgast, Ç. Kurdak, K. Sun, J.W. Allen, D.-J. Kim, Z. Fisk, Low-temperature surface conduction in the Kondo insulator SmB_6, Phys. Rev. B 88 (2013) 180405, http://dx.doi.org/10.1103/PhysRevB.88.180405, URL https://link.aps.org/doi/10.1103/PhysRevB.88.180405.

[8] L. Kouwenhoven, L. Glazman, Revival of the Kondo effect, Phys. World 14 (1) (2001) 33.

[9] T. Kasuya, K. Takegahara, T. Fujita, T. Tanaka, E. Bannai, Valence fluctuating state in SmB6, Le J. Phys. Colloques 40 (C5) (1979) C5–308.

[10] S. Nozawa, T. Tsukamoto, K. Kanai, T. Haruna, S. Shin, S. Kunii, Ultrahigh-resolution and angle-resolved photoemission study of SmB6, J. Phys. Chem. Solids 63 (6–8) (2002) 1223–1226.

[11] P. Nyhus, S.L. Cooper, Z. Fisk, J. Sarrao, Low-energy excitations of the correlation-gap insulator SmB_6:ffA light-scattering study, Phys. Rev. B 55 (1997) 12488–12496, http://dx.doi.org/10.1103/PhysRevB.55.12488, URL https://link.aps.org/doi/10.1103/PhysRevB.55.12488.

[12] W. Ruan, C. Ye, M. Guo, F. Chen, X. Chen, G.-M. Zhang, Y. Wang, Emergence of a coherent in-gap state in the SmB_6 Kondo insulator revealed by scanning tunneling spectroscopy, Phys. Rev. Lett. 112 (2014) 136401, http://dx.doi.org/10.1103/PhysRevLett.112.136401, URL https://link.aps.org/doi/10.1103/PhysRevLett.112.136401.

[13] A. Barla, J. Derr, J.P. Sanchez, B. Salce, G. Lapertot, B.P. Doyle, R. Rüffer, R. Lengsdorf, M.M. Abd-Elmeguid, J. Flouquet, High-pressure ground state of SmB_6: Electronic conduction and long range magnetic order, Phys. Rev. Lett. 94 (2005) 166401, http://dx.doi.org/10.1103/PhysRevLett.94.166401, URL https://link.aps.org/doi/10.1103/PhysRevLett.94.166401.

[14] J. Derr, G. Knebel, D. Braithwaite, B. Salce, J. Flouquet, K. Flachbart, S. Gabáni, N. Shitsevalova, From unconventional insulating behavior towards conventional magnetism in the intermediate-valence compound SmB_6, Phys. Rev. B 77 (2008) 193107, http://dx.doi.org/10.1103/PhysRevB.77.193107, URL https://link.aps.org/doi/10.1103/PhysRevB.77.193107.

[15] Y. Zhou, Q. Wu, P.F. Rosa, R. Yu, J. Guo, W. Yi, S. Zhang, Z. Wang, H. Wang, S. Cai, K. Yang, A. Li, Z. Jiang, S. Zhang, X. Wei, Y. Huang, P. Sun, Y. feng Yang, Z. Fisk, Q. Si, Z. Zhao, L. Sun, Quantum phase transition and destruction of Kondo effect in pressurized SmB6, Sci. Bull. 62 (21) (2017) 1439–1444, http://dx.doi.org/10.1016/j.scib.2017.10.008, URL https://www.sciencedirect.com/science/article/pii/S2095927317305248.

[16] J.W. Allen, L.I. Johansson, I. Lindau, S.B. Hagstrom, Surface mixed valence in Sm and SmB_6, Phys. Rev. B 21 (1980) 1335–1343, http://dx.doi.org/10.1103/PhysRevB.21.1335, URL https://link.aps.org/doi/10.1103/PhysRevB.21.1335.

[17] Y. Utsumi, D. Kasinathan, K.-T. Ko, S. Agrestini, M. Haverkort, S. Wirth, Y. Wu, K. Tsuei, D. Kim, Z. Fisk, et al., Bulk and surface electronic properties of SmB 6: A hard x-ray photoelectron spectroscopy study, Phys. Rev. B 96 (15) (2017) 155130.

[18] P. Lutz, M. Thees, T. Peixoto, B. Kang, B. Cho, C.H. Min, F. Reinert, Valence characterisation of the subsurface region in, Phil. Mag. 96 (31) (2016) 3307–3321.

[19] J.-m. Tarascon, Y. Isikawa, B. Chevalier, J. Etourneau, P. Hagenmuller, M. Kasaya, Temperature dependence of the samarium oxidation state in SmB6 and Sm1-xLaxB6, J. Physique 41 (10) (1980) 1141–1145.

[20] E. Beaurepaire, J. Kappler, G. Krill, X-ray-absorption near-edge structure study in mixed-valent samarium systems, Phys. Rev. B 41 (10) (1990) 6768.

[21] M. Mizumaki, S. Tsutsui, F. Iga, Temperature dependence of Sm valence in SmB6 studied by X-ray absorption spectroscopy, in: Journal of Physics: Conference Series, Vol. 176, IOP Publishing, 2009, 012034.

[22] K. Chen, T. Weng, G. Schmerber, V. Gurin, J.-P. Kappler, Q. Kong, F. Baudelet, A. Polian, L. Nataf, Surface-and pressure-induced bulk Kondo breakdown in SmB 6, Phys. Rev. B 97 (23) (2018) 235153.

[23] N. Emi, N. Kawamura, M. Mizumaki, T. Koyama, N. Ishimatsu, G. Pristáš, T. Kagayama, K. Shimizu, Y. Osanai, F. Iga, et al., Kondo-like behavior near the magnetic instability in SmB 6: Temperature and pressure dependences of the Sm valence, Phys. Rev. B 97 (16) (2018) 161116.

[24] O. Mathon, A. Beteva, J. Borrel, D. Bugnazet, S. Gatla, R. Hino, I. Kantor, T. Mairs, M. Munoz, S. Pasternak, et al., The time-resolved and extreme conditions XAS (TEXAS) facility at the European Synchrotron Radiation Facility: the general-purpose EXAFS bending-magnet beamline BM23, J. Synchrotron Radiat. 22 (6) (2015) 1548–1554.

[25] T. Irifune, A. Kurio, S. Sakamoto, T. Inoue, H. Sumiya, Materials: Ultrahard polycrystalline diamond from graphite, Nature 421 (6923) (2003) 599.

[26] N. Ishimatsu, K. Matsumoto, H. Maruyama, N. Kawamura, M. Mizumaki, H. Sumiya, T. Irifune, Glitch-free X-ray absorption spectrum under high pressure obtained using nano-polycrystalline diamond anvils, J. Synchrotron Radiat. 19 (5) (2012) 768–772.

[27] F. Datchi, A. Dewaele, P. Loubeyre, R. Letoullec, Y. Le Godec, B. Canny, Optical pressure sensors for high-pressure–high-temperature studies in a diamond anvil cell, High Press. Res. 27 (4) (2007) 447–463.

[28] N. Tateiwa, Y. Haga, Evaluations of pressure-transmitting media for cryogenic experiments with diamond anvil cell, Rev. Sci. Instrum. 80 (12) (2009).

[29] R.M. Martin, J.B. Boyce, J.W. Allen, F. Holtzberg, Extended X-Ray-absorption fine-structure studies of electron-lattice correlations in mixed-valence $Sm_{0.75}Y_{0.25}S$, Phys. Rev. Lett. 44 (1980) 1275–1278, http://dx.doi.org/10.1103/PhysRevLett.44.1275, URL https://link.aps.org/doi/10.1103/PhysRevLett.44.1275.

[30] B. Lengeler, G. Materlik, J.E. Müller, *L*-Edge x-ray absorption spectra of γ – andα – cerium, Phys. Rev. B 28 (1983) 2276–2278, http://dx.doi.org/10.1103/PhysRevB.28.2276, URL https://link.aps.org/doi/10.1103/PhysRevB.28.2276.

[31] G. Krill, J. Kappler, M. Ravet, C. Godart, J. Senateur, Local environment effects in mixed valent rare-earth systems studied by EXAFS, J. Magn. Magn. Mater. 47 (1985) 190–196.

[32] A. Filipponi, A. Di Cicco, C.R. Natoli, X-ray absorption spectroscopy and n-body distribution functions in condensed matter (I): theory, Phys. Rev. B 52 (1995) 15122–15134.

[33] A. Filipponi, A. Di Cicco, X-ray absorption spectroscopy and n-body distribution functions in condensed matter (II): data-analysis and applications, Phys. Rev. B 52 (1995) 15135.

[34] N. Brandt, V. Moshchalkov, S. Pashkevich, M. Vybornov, M. Semenov, T. Kolobyanina, E. Konovalova, Y.B. Paderno, High pressure studies of cerium hexaboride, Solid State Commun. 56 (11) (1985) 937–941.

[35] V. Trounov, A. Malyshev, D.Y. Chernyshov, M. Korsukova, V. Gurin, L. Aslanov, V. Chernyshev, Temperature dependences of the parameters of atoms in the crystal structure of the intermediate-valence semiconductor SmB6: investigation by high-resolution powder neutron diffraction, J. Phys.: Condens. Matter. 5 (16) (1993) 2479.

[36] K. Chen, Y. Mijiti, S. Agrestini, S.-C. Liao, X. Li, J. Zhou, A. Di Cicco, F. Baudelet, L.H. Tjeng, Z. Hu, Valence state of Pb in transition metal perovskites PbTMO3 (TM=Ti, Ni) determined from X-Ray absorption near-edge spectroscopy, Phys. Status Solidi (b) 255 (6) (2018) 1800014.

[37] J. García, G. Subías, J. Blasco, XAS studies on mixed valence oxides, in: X-Ray Absorption and X-Ray Emission Spectroscopy: Theory and Applications, Wiley Online Library, 2016, pp. 459–484.

[38] E. Mijit, K. Chen, J.E.F.S. Rodrigues, Z. Hu, L. Nataf, A. Trapananti, A. Di Cicco, F. Baudelet, Crystal and electronic structure of Co_3O_4 spinel under pressure probed by XANES and Raman spectroscopy, Phys. Rev. B 103 (2021) 024105, http://dx.doi.org/10.1103/PhysRevB.103.024105, URL https://link.aps.org/doi/10.1103/PhysRevB.103.024105.

[39] C. Rao, D. Sarma, P. Sarode, E. Sampathkumaran, L. Gupta, R. Vijayaraghavan, Valence fluctuation in some Yb intermetallics by X-ray photoemission and X-ray absorption, Chem. Phys. Lett. 76 (3) (1980) 413–415.

[40] H. Launois, M. Rawiso, E. Holland-Moritz, R. Pott, D. Wohlleben, X-Ray absorption study of mixed-valence TmSe, Phys. Rev. Lett. 44 (1980) 1271–1275, http://dx.doi.org/10.1103/PhysRevLett.44.1271, URL https://link.aps.org/doi/10.1103/PhysRevLett.44.1271.

[41] K. Matsubayashi, T. Hirayama, T. Yamashita, S. Ohara, N. Kawamura, M. Mizumaki, N. Ishimatsu, S. Watanabe, K. Kitagawa, Y. Uwatoko, Pressure-induced valence crossover and novel metamagnetic behavior near the antiferromagnetic quantum phase transition of $YbNi_3Ga_9$, Phys. Rev. Lett. 114 (2015) 086401, http://dx.doi.org/10.1103/PhysRevLett.114.086401, URL https://link.aps.org/doi/10.1103/PhysRevLett.114.086401.

[42] J. Yamaguchi, A. Sekiyama, M. Kimura, H. Sugiyama, Y. Tomida, G. Funabashi, S. Komori, T. Balashov, W. Wulfhekel, T. Ito, et al., Different evolution of the intrinsic gap in strongly correlated SmB6 in contrast to YbB12, New J. Phys. 15 (4) (2013) 043042.

[43] J. Jiang, S. Li, T. Zhang, Z. Sun, F. Chen, Z. Ye, M. Xu, Q. Ge, S. Tan, X. Niu, et al., Observation of possible topological in-gap surface states in the Kondo insulator SmB6 by photoemission, Nat. Commun. 4 (1) (2013) 1–8.

[44] K.A. Gschneidner, J.-C.G. Bunzli, V.K. Pecharsky, Handbook on the Physics and Chemistry of Rare Earths, Vol. 34, Elsevier, 2005.

[45] B.L. Davis, L.H. Adams, X-ray diffraction evidence for a critical end point for cerium I and cerium II, J. Phys. Chem. Solids 25 (4) (1964) 379–388.

[46] J.L. Sarrao, C.D. Immer, C.L. Benton, Z. Fisk, J.M. Lawrence, D. Mandrus, J.D. Thompson, Evolution from first-order valence transition to heavy-fermion behavior in $YbIn_{1-x}Ag_xCu_4$, Phys. Rev. B 54 (1996) 12207–12211, http://dx.doi.org/10.1103/PhysRevB.54.12207, URL https://link.aps.org/doi/10.1103/PhysRevB.54.12207.

[47] S. Watanabe, A. Tsuruta, K. Miyake, J. Flouquet, Valence fluctuations revealed by magnetic field and pressure scans: Comparison with experiments in YbXCu4 (X=In, Ag, Cd) and CeYIn5 (Y=Ir, Rh), J. Phys. Soc. Japan 78 (10) (2009) 104706.

[48] S. Seiro, C. Geibel, From stable divalent to valence-fluctuating behaviour in Eu (Rh1- xIrx) 2Si2 single crystals, J. Phys.: Condens. Matter. 23 (37) (2011) 375601.

[49] F. Honda, K. Okauchi, A. Nakamura, D. Li, D. Aoki, H. Akamine, Y. Ashitomi, M. Hedo, T. Nakama, Y. Ōnuki, Pressure-induced valence transition and characteristic electronic states in EuRh2Si2, J. Phys. Soc. Jpn 85 (6) (2016) 063701.

[50] J.-T. Zhuang, X.-J. Zheng, Z.-Y. Wang, X. Ming, H. Li, Y. Liu, H.-F. Song, Valence transition in topological Kondo insulator, J. Phys.: Condens. Matter. 32 (3) (2020) 035602.

[51] C. Natoli, Distance dependence of continuum and bound state of excitonic resonances in X-ray absorption near edge structure (XANES), in: EXAFS and Near Edge Structure III, Springer, 1984, pp. 38–42.

[52] N.P. Butch, J. Paglione, P. Chow, Y. Xiao, C.A. Marianetti, C.H. Booth, J.R. Jeffries, Pressure-resistant intermediate valence in the Kondo insulator SmB_6, Phys. Rev. Lett. 116 (2016) 156401, http://dx.doi.org/10.1103/PhysRevLett.116.156401, URL https://link.aps.org/doi/10.1103/PhysRevLett.116.156401.

[53] A. Fernandez-Pañella, V. Balédent, D. Braithwaite, L. Paolasini, R. Verbeni, G. Lapertot, J.-P. Rueff, Valence instability of $YbCu_2Si_2$ through its magnetic quantum critical point, Phys. Rev. B 86 (2012) 125104, http://dx.doi.org/10.1103/PhysRevB.86.125104, URL https://link.aps.org/doi/10.1103/PhysRevB.86.125104.

[54] H. Yamaoka, I. Jarrige, N. Tsujii, J.-F. Lin, N. Hiraoka, H. Ishii, K.-D. Tsuei, Temperature and pressure-induced valence transitions in $YbNi_2Ge_2$ and $YbPd_2Si_2$, Phys. Rev. B 82 (2010) 035111, http://dx.doi.org/10.1103/PhysRevB.82.035111, URL https://link.aps.org/doi/10.1103/PhysRevB.82.035111.

[55] H. Yamaoka, N. Tsujii, Y. Utsumi, H. Sato, I. Jarrige, Y. Yamamoto, J.-F. Lin, N. Hiraoka, H. Ishii, K.-D. Tsuei, J. Mizuki, Valence transitions in the heavy-fermion compound YbCuAl as a function of temperature and pressure, Phys. Rev. B 87 (2013) 205120, http://dx.doi.org/10.1103/PhysRevB.87.205120, URL https://link.aps.org/doi/10.1103/PhysRevB.87.205120.

[56] H. Yamaoka, Y. Zekko, A. Kotani, I. Jarrige, N. Tsujii, J.-F. Lin, J. Mizuki, H. Abe, H. Kitazawa, N. Hiraoka, H. Ishii, K.-D. Tsuei, Electronic transitions in $CePd_2Si_2$ studied by resonant x-ray emission spectroscopy at high pressures and low temperatures, Phys. Rev. B 86 (2012) 235131, http://dx.doi.org/10.1103/PhysRevB.86.235131, URL https://link.aps.org/doi/10.1103/PhysRevB.86.235131.

[57] H. Yamaoka, Y. Ikeda, I. Jarrige, N. Tsujii, Y. Zekko, Y. Yamamoto, J. Mizuki, J.-F. Lin, N. Hiraoka, H. Ishii, K.-D. Tsuei, T.C. Kobayashi, F. Honda, Y. Ōnuki, Role of valence fluctuations in the superconductivity of Ce122 compounds, Phys. Rev. Lett. 113 (2014) 086403, http://dx.doi.org/10.1103/PhysRevLett.113.086403, URL https://link.aps.org/doi/10.1103/PhysRevLett.113.086403.